

Flexural Behavior of Spun Concrete Poles Reinforced with CFRP Bars

Ashraf M. Shalaby, Fouad H. Fouad, and Ronald Albanese

INTRODUCTION

Carbon fiber reinforced polymer (CFRP) reinforcement is showing immense potential in the civil engineering applications as an alternative to traditional steel reinforcement because of their unique properties. CFRP has high strength, light weight, non conductive, non corrosive and non magnetic. It is due to the improved durability of CFRP reinforced concrete that CFRP is gaining considerable use and attention by those who are working in the reinforced concrete field.

Research work has been performed on the use of CFRP in concrete structures. Most of the research has focused on the traditional rectangular and tee cross sectional shapes that are commonly used in reinforced concrete structures, such as buildings and bridges. Very limited information, however, is available in the literature on circular concrete sections reinforced with CFRP^{1,2}.

Members with circular cross sections are commonly used in the precast industry for a variety of products such as poles, piles, pipes, and most recently columns for buildings and bridge piers. Round spun concrete poles are used in supporting electric transmission lines, communication towers, stadium lighting, and a variety of other applications. The round cross-section, which is dictated by the manufacturing process in the case of spun concrete, offers a number of advantages including a smooth finish, denser concrete material, reduced wind pressure, and improved aesthetics^{3,4,5}.

This paper presents the results of an experimental and analytical program that was conducted at the University of Alabama at Birmingham to study the flexural behavior of spun concrete poles reinforced with CFRP bars.

EXPERIMENTAL PROGRAM

The main objective of the experimental program was to evaluate the flexural behavior of spun concrete poles reinforced with CFRP bars. Two sets of prototype pole specimens reinforced with CFRP bars were manufactured under normal precast concrete plant conditions. All specimens were identical except for the reinforcement scheme. The first set of specimens

consisted of two poles each reinforced with 6 CFRP longitudinal bars. One of the specimens used steel spiral reinforcement for confinement and the second specimen used a CFRP grid. The poles of the second set of test specimens were each reinforced with 12 CFRP longitudinal bars, but otherwise identical to the first set of test specimens in geometry and confinement reinforcement.

Materials Properties

The spun concrete test poles were produced of a high-strength concrete mix at the Valmont-Newmark Company spun concrete pole facility in Alabama. The 28-day compressive strength of the concrete was 11,000 psi (75.84 MPa). The CFRP reinforcing bars used were provided by Hughes Brothers, Inc. under the commercial name of Aslan 200 (Figure 1). Aslan 200 is a solid rod specially treated to enhance bond to Portland cement. The physical properties of the Aslan 200 are given in Table 1. The CFRP grid used as transverse confining reinforcement was provided by TechFab LLC under the commercial name of C-GRID (Figure 2). C-GRID is a high performance reinforcement made by bonding ultra-high strength carbon tows with epoxy resin in a controlled factory environment. The manufacturer designation for the C-GRID used is C50-2.9 x 2.9 in English designation and is C50-72 x 72 in Metric designation. The grid is composed of a square mesh of carbon strands spaced at 2.9 in (72 mm) each way. Typical C-GRID properties and the physical properties of the CFRP strand are given in Table 2 and Table 3 respectively. In some specimens steel wire 3/16" in diameter per ASTM A82⁶ was used as spiral for the transverse reinforcement.

Specimen Dimensions and Reinforcement Details

All test specimens were identical in geometry. Specimens were 20 ft long (6096 mm) with an outer diameter of 8.91 in (226 mm) and 13.23 in (336 mm) at the tip and butt ends, respectively, which provides an outside slope of 1.8% (0.216 in/ft). The inner diameters were 3.91 in (99 mm) and 7.75 in (191 mm) for the tip and butt ends, respectively, with an inside slope of 1.6% (0.192 in/ft). The wall thickness was 2.5 in (63.50 mm) and 2.74 in (69.60 mm) at the tip and butt ends, respectively. The test specimens' dimensions are shown in Figure 3. Although larger size of specimens could have been used, the size of the specimen was chosen to allow for easy transportation from the production plant to the structural laboratory at the University of Alabama at Birmingham. The CFRP bars were 3/8 in (9 mm) in diameter and were distributed uniformly

around the cross section. Steel spirals or CFRP grid were used for confinement as shown in Figure 4, and Figure 5. The steel spirals had a wire diameter of 3/16 in (5 mm) with a pitch of 3.0 in (75 mm) center-to-center, and a concrete cover of 0.75 in (19 mm). Figure 6 shows the cross-sectional and reinforcement details of the poles. Table 4 provides a summary of the geometry and reinforcement details for the test specimens. In Table 4, the first two digits of the specimen ID following the letter “P” represent the pole number, the third and fourth digits represent the number of CFRP bars used, the letters “SS” indicate poles confined with steel spirals, and the letters “CG” indicate the poles confined with the C-GRID.

Test Setup and Procedure

A schematic diagram of the test setup is shown on Figure 7. A photograph of test setup is shown in Figure 8. Figure 9 shows the detail at the end fixation. The pole specimen rested on two supports. The first support was located at the pole’s butt end, and the second support which served as the fulcrum, was located 3.0 ft (1000 mm) from the pole’s butt end. The distance to the fulcrum point was chosen to represent the typical foundation embedment length used in practice, which is approximately 10% of the overall pole length plus one foot. The steel supports were designed and manufactured specifically to sustain the reactions from the load applied to the pole. The two supports were equipped with two semicircular collars, on which the poles were placed and clamped (Figure 8) to restrain the poles against lateral movement.

The load was applied at a distance of 1.0 ft (305 mm) from the tip of the pole. The lever arm, measured to the centerline of the first restraining support (fulcrum point) was 16.0 ft (4877 mm). The load was applied using a manual chain hoist connected to a tension load cell and hooked to the trolley crane of the laboratory, as shown in Figure 10.

Two sets of strain gages each consisting of four gages were installed along the circumference of the pole at distances of 6 in (150 mm) and 18 in (450 mm) from the fulcrum support, as shown in Figure 11. For each set of strain gages, two gages were located at the horizontal centerline of the cross-section of the pole where the maximum compressive and tensile stresses occur, and the other two gages were located at the vertical centerline (the neutral axis) of the cross-section of the pole.

The tip deflection was recorded by two means. The first was a scale that was attached to the test frame near the tip of the pole, and the second was a tape that was connected to the pole as

shown in Figure 12. After first cracking of the specimen, the crack width was measured at each load increment using concrete comparators. The strain gages and the load cell readings were recorded via a data acquisition system and the data transferred to a computer for analysis.

Two Linear Variable Differential Transformers (LVDTs) were installed adjacent to the supports of the test pole as shown in Figure 13 to record any movement that may occur at the supports. The readings would be used to correct the measured deflection at the tip of the pole.

The load was applied in increments of about 100 pounds. There was a pause after each load increment to allow for reading deflections, inspect for cracks, and to observe any structural distress that might have occurred. Two of the test specimens were subjected to loading and unloading cycles to study the elastic and plastic deformation of the poles and inspect cracks after unloading. Pole P02-6CG was loaded up to 80% of the designed ultimate load and the load was totally released, then the pole was reloaded again up to failure. Pole P04-12CG was loaded up to 50% of the designed ultimate load, load was released, reloaded up to 80%, and load was released, and then reloaded up to failure.

Test Results

A summary of the test results is given in Table 5. It can be seen that the poles reinforced with 6 CFRP bars provided higher deflection values, at failure load, than the pole reinforced with 12 CFRP bars. The deflection of the poles was about 12% and 10% of the free length of the poles for the poles reinforced with 6 CFRP bars and 12 CFRP bars, respectively. Also, it can be seen that the poles confined with the C-GRID failed at higher load values than specimens confined with steel spirals. The failure load of the poles confined with the C-GRID was higher than the poles confined with steel spirals by 8% and 24% for the poles reinforced with 6 CFRP bars and 12 CFRP bars, respectively. The reasons for the differences are explained later in this paper.

Deflection - Figure 14 shows the load deflection curves of all specimens from zero loading and up to failure. For a closer look at the curves, Figure 15 provides a plot of the load deflection curves from zero loading up to a load of 1700 lbs (7.56 kN). From Figure 15, it can be seen that all specimens deflected linearly with load and had almost the same deflection values starting from a zero load and up to a load of about 750 lbs (3.34 kN), which corresponds to the average cracking load of the poles. Following the cracking load and up to a load of 1500 lbs (6.67 kN), the poles started to deflect nonlinearly with load, but still the deflection curves almost coincided

with each other. In this nonlinear stage, the cracks start forming in several locations along the pole length. At loads greater than 1500 lbs (6.67 kN), there were no more cracks formed and the load deflection behavior became linear again, but the slope of the line was significantly smaller than the slope before cracking. The slope of this linear portion was different for the specimens. From Figure 14, it can be seen that the poles reinforced with 12 CFRP bars had higher stiffness than the poles reinforced with 6 CFRP bars. It can also be observed that the poles confined with the C-GRID had higher stiffness than the poles confined with steel stirrups, which shows a contribution of the C-GRID to the increase in stiffness after cracking.

Failure mode - Two types of failure modes were observed, as shown in Table 6. For poles confined with steel spirals, diagonal shear cracks formed between the two supports prior to failure, and at failure the concrete crushed explosively in compression near the fulcrum support independent of the diagonal shear cracks, as shown in Figure 16. For poles confined with the C-GRID, diagonal shear cracks formed between the two supports prior to the failure, and as the load increased, the diagonal shear cracks widened and extended to the top compression fibers of the pole, and a sudden failure took place as this crack joined the crushed concrete zone, as shown in Figure 17. The failure of these poles was also characterized by the slippage of the CFRP bars at failure, as shown in Figure 18. This slippage is due to the destruction of the bond between the longitudinal bars and the surrounding concrete at the support region, which frequently occurs in conjunction with the flexural shear failure mode.

After reaching the ultimate load and unloading the poles, it was observed that pole P01-6SS underwent a permanent cracking and deflection. This permanent cracking and deflection could be due to the low reinforcement ratio used in this pole. The lower reinforcement ratio results in subjecting the reinforcement bars to higher strains and stresses which correspondingly results in wider crack widths. With the wide cracks, and the difference between the modulus of elasticity of concrete and CFRP bars, the cracks were irrecoverable, and the pole underwent permanent cracking and deflection. On the other hand, for the pole P03-12SS, all the cracks were closed, leaving some hair-line cracks, and the residual deflection recorded was very low, and this could be contributed to the number of bars used in this pole. With more bars, lower strains and stresses were transferred from the concrete to the reinforcement, which correspondingly results in smaller crack widths that can recover after unloading.

Crack spacing - Figure 19 shows the crack pattern along the length of the pole P01-6SS after reaching the ultimate load and unloading the pole. The residual crack width for this pole was 0.04 in (1.0 mm) and the crack was located at one foot (305 mm) from the fulcrum support toward the tip end of the pole on the tension side. Other residual cracks in this region were about 0.035 in (0.875 mm) and were spaced at 4 in (100 mm). Moving toward the middle of the pole up to 10 ft (3050 mm) from the butt end, the residual crack width decreased measuring an average of 0.02 in (0.5 mm); however, the crack spacing ranged from 3 to 4 in (75 to 100 mm). For the second half of the pole, starting at 10 ft (3050 mm) from the butt end and up to five feet (1525 mm) from the tip end, the residual crack width measured an average of 0.007 in (0.18 mm), with crack spacing of 6 in (150 mm). There was no cracking observed for the rest of the pole. For pole P02-6CG, after reaching the ultimate load and unloading the pole, all of the cracks were closed, leaving only hair-line cracks. Although there were not as many cracks as with pole P01-6SS, the cracks for pole P02-6CG were spaced every 4.0 in (100 mm), starting from the fulcrum support, on the tension side, and up to 10 ft (3050 mm) from the butt end.

Figure 20 shows the crack pattern along the length of pole P03-12SS. All of the cracks left after unloading were hair-line cracks that were hardly seen, and they were distributed at 4 in (100 mm), starting from the fulcrum support and up to up to 10 ft (3050 mm) from the butt end. For the rest of the pole, there were no cracks observed. The crack distribution for pole P04-12CG was similar to the crack distribution of pole P03-12SS.

From these observations, it can be concluded that the number of reinforcing bars in the pole does not have a significant effect on the crack spacing.

Crack width - Figure 21 shows the crack width versus loading for the pole P02-6CG at two feet (610 mm) from the fulcrum support where the first crack was formed, and it also shows the crack width versus loading at one foot (305 mm) from the fulcrum support for the poles reinforced with 12 CFRP bars. From this figure it could be seen that the crack widths for the pole reinforced with 6 CFRP bars were much wider than those for the poles reinforced with 12 CFRP bars. Also, for pole P02-6CG, the crack widths were significantly increased by loading and unloading, whereas there was no difference in the crack widths for pole P04-12CG when subject to loading and unloading cycles. From these observations, it could be concluded that the number of bars significantly affects the crack widths of the poles.

Figure 21 also shows that the crack widths for the pole P04-12CG confined with the C-GRID is much less than the pole P03-12SS confined with steel spirals. Confining the pole with CFRP grid means that the pole has CFRP strands in the circumferential and longitudinal directions. The CFRP strands in the longitudinal direction being spaced at 2.9 in (72 mm), and having a small cross-sectional area will result in a gradual transfer of the concrete tensile stress to the reinforcing bars which correspondingly will result in a significant reduction in the crack widths of the pole. It was obvious from Figure 21 that the C-GRID significantly decreased the crack widths of the poles.

The significant reduction in the crack widths for poles confined with C-GRID, as compared to poles confined with steel spirals, results in an increase in the area of concrete subjected to compression. The tensile force in the CFRP bars will also increase to balance the compression force. Accordingly, there will be a corresponding increase in the ultimate moment capacity. This explains the differences in the ultimate capacities, shown in Table 5 and mentioned above, between the poles confined with the C-GRID and that confined with steel spirals.

ANALYTICAL STUDY

Theoretical studies were performed prior to testing to predict the behavior of the spun concrete poles reinforced with CFRP and compare to the experimental results. Design equations available in the literature and design guidelines for concrete poles and concrete structures reinforced with CFRP^{7,8,9,10,11,12} were evaluated and modified to estimate the flexural capacity, deflection, and crack widths of the spun pole test specimens.

Ultimate Moment Capacity

The ultimate moment capacity of the poles was determined based on strain compatibility and the internal force equilibrium (Figure 22) as follows:

$$M_u = \sum_{i=1}^n e_i A_{fi} f_{fei} + C_c (c - Kc)$$

$$e_i = d_i - c$$

$$f_{fei} \leq f_{fu}$$

Where A_{fi} and f_{fei} are the area and stress of the i^{th} reinforcement, respectively. c is the location of the neutral axis measured from the extreme compression fiber of the pole, Kc is the position of the centroid of the stress block, d_i is the distance of the i^{th} reinforcement from the extreme compression fiber, e_i is the distance of the i^{th} reinforcement to the neutral axis, and f_{fu} is the ultimate strength of the CFRP bars. c is calculated using the trial and error iterations method to balance the compression and tension forces acting on the cross-section, therefore, a spreadsheet were developed to facilitate the analysis and design process.

Unlike traditional steel reinforcement, CFRP is a linearly elastic material up to failure and does not have a yielding point, which implies a sudden failure once the CFRP bar reaches its ultimate strength.

Cracking Moment Capacity

Cracking starts when the tensile stress in the extreme fiber of the concrete reaches its modulus of rupture. The cracking moment can be computed by elastic theory to predict the behavior of poles and is calculated, as proposed by ACI 318-08⁷, using the following relationships:

$$M_{cr} = \frac{f_r I_g}{y_t}$$

$$f_r = 7.5\sqrt{f'_c}$$

Where M_{cr} is the cracking moment, f_r is the modulus of rupture of concrete, f'_c is the cylinder compressive strength of concrete at 28 days, I_g is the gross moment of inertia of the section, and y_t is the distance from the centroidal axis to the extreme tensile fiber of the section.

Deflection

Theoretical deflection calculations were performed using the virtual work method as follows:

$$\Delta = \int_0^L \frac{M \cdot x}{EI} dx$$

Where M is the applied moment, x is the distance from the support, E is the modulus of elasticity of concrete, I is the moment of inertia, and L is the length of the pole. Before cracking of the concrete section, the gross moment of inertia (I_g) is used to calculate the deflection, however after cracking; the effective moment of inertia (I_e) is used. Noteworthy to mention that concrete poles are tapered structures, so their moment of inertia is variable along the pole length.

Many approaches have been proposed to calculate the effective moment of inertia for concrete structures reinforced with FRP bars; however in this study the approach presented by Bischoff and Scanlon¹⁰ was used to calculate the deflection of the tested specimens. Reduction factor, as proposed by Shalaby¹³, was applied to account for the shape difference and reinforcement alignment between rectangular and circular concrete sections. The following equation was used to calculate the effective moment of inertia (I_e):

$$I_e = \frac{0.83I_{cr}}{\left(1 - \eta \left(\frac{M_{cr}}{M_a}\right)^2\right)} \leq I_g$$

$$\eta = 1 - \frac{0.83I_{cr}}{I_g}$$

Crack Width

The following ACI 440.1R-03 equation was used to calculate the crack width of spun concrete poles reinforced with CFRP.

$$w = \frac{2200}{E_f} \beta \cdot k_b \cdot f_{f_{ei}} \cdot \sqrt[3]{d_c \cdot A}$$

$$\beta = \frac{e_t}{e_i}$$

Where w is the crack width in mils, d_c and A are as shown in Figure 23, and k_b is a bond coefficient assumed to be 1.0 for this study. A bond coefficient of 1.0 means that the CFRP bars have the same bond as the traditional steel reinforcement, a higher value for the bond coefficient means higher bond, and a smaller value means less bond. E_f is the tensile modulus of elasticity of CFRP bars, and $f_{f_{ei}}$ is the stress on the i^{th} reinforcement.

The equation was developed for a rectangular concrete section with single layer of reinforcement; however, spun concrete poles are round, and the reinforcement is aligned around the cross-section, therefore, the definition of the effective tension area of concrete A was modified to account for the shape difference and reinforcement alignment between rectangular and circular concrete sections. In rectangular concrete sections with single layer of reinforcement, the effective tension area of concrete A is defined as the area of concrete having the same centroid as that of tensile reinforcement, divided by the number of bars. In this study, the effective tension area of concrete A was defined as the area of concrete having the same centroid as that of the tensile reinforcement farthest from the neutral axis (Figure 23).

RESULTS AND DISCUSSION

Cracking and Ultimate Moments

Table 7 shows the theoretical and experimental cracking moments of the poles. Since the cracking moment depends mainly on the modulus of rupture of the concrete, and the reinforcement ratio has a small effect, the average cracking moment of the four poles was compared to the theoretical cracking moment. The test yielded an average cracking moment of 12.17 kips.ft (16.50 kN.m), versus the theoretical cracking moment of 11.46 kips.ft (15.54 kN.m). The difference is only 6% between the theoretical and experimental values, which indicates comparable results. Table 8 shows the theoretical and experimental ultimate moments of the poles. The theoretical ultimate moment capacity was very close to the experimental ultimate moment for pole P01-6SS with only 2% difference. For pole P03-12SS the theoretical ultimate moment capacity was higher than the experimental by 9%. For the other two poles, confined with the C-GRID (P02-6CG and P04-12CG), the experimental ultimate moment capacities was higher than the theoretical by 9% and 12%, respectively. This increase may be attributed to the confinement provided by the C-GRID as well as the strands of the C-GRID in the longitudinal direction of the pole, which will contribute to the increase in the ultimate capacity of the poles.

Deflection

Figures 24 and 25 shows a comparison between the load-deflection curves obtained from the experimental data and those developed using the analytical equations discussed above. From

these figures, it could be seen that the theoretical and experimental curves are in very close agreement. The good correlation will allow the prediction of deflections at service and ultimate loads with a high degree of accuracy.

Crack Width

Table 9 shows the maximum crack width measured during the test compared to that calculated using the ACI 440.1R-03 equation. From this table we can see that there is a significant difference between the test and calculated values for all of the poles except P03-12SS. For pole P01-6SS, the crack width was measured after reaching ultimate load and unloading the pole, and moving it from the test frame, so this crack width is the permanent crack width that remains after unloading, and does not represent the actual crack width during the test. For pole P02-6CG, the crack width was calculated at several load intervals that correspond to the experimental data recorded. At a 70% of the ultimate load, the equation used to calculate the crack width underestimates the crack width of the pole by about 15%; however, Figure 26 shows that at lower loads the calculated crack width is comparable to the crack width measured during the test.

Figure 27 shows the load crack width curve for the poles reinforced with 12 CFRP bars. It can be seen that for pole P03-12SS the ACI 440.1R-03 equation correlates well with the experimental results, especially for higher loads. For lower loads, the correlation is not as much as for higher loads, and this contradicts with pole P02-6CG. For pole P04-12CG, it can be seen from Figure 27 that the measured crack width during loading is significantly different from the measured crack width of pole P03-12SS and the theoretical calculations.

From this discussion, it could be concluded that using the ACI 440.1R-03 equation to estimate the crack width of spun concrete poles reinforced with CFRP bars will give misleading results. Additional testing is necessary to come up with a suitable formula that can be used to calculate the crack width of spun concrete poles reinforced with CFRP bars.

CONCLUSIONS

The conclusions drawn out from this study can be summarized as follows:

1. Concrete poles reinforced with CFRP bars showed satisfactory flexural behavior. Ductility was demonstrated by the significant amount of deflection, about 12% of the free length of the pole, prior to failure.

2. The ultimate moment capacity of spun concrete pole cross sections reinforced with CFRP bars calculated using the proposed equations compared well with the experimental results.
3. The flexural crack spacing at failure was approximately 3.5 inches, uniformly distributed along the pole length (from the fulcrum point up to 10 ft (3050 mm) from the butt end of the pole). The number of reinforcing bars in the pole did not have a significant effect on crack spacing.
4. The number of reinforcing bars in a pole significantly affects the crack width of the pole. The crack widths of the poles reinforced with 6 CFRP bars were much wider than those for the poles reinforced with 12 CFRP bars. Also, the crack widths were significantly increased by loading and unloading for poles reinforced with 6 CFRP bars, whereas there was no difference in the crack widths for poles reinforced with 12 CFRP bars and subjected to loading and unloading cycles.
5. Confining the poles with C-GRID significantly decreased the crack width of the poles; with the poles having the same reinforcement ratio, the crack width for the poles confined with the C-GRID was decreased by about 40% prior to failure, as compared to the poles confined with steel spirals.
6. Confining the poles with C-GRID affected the failure mode of the poles. The poles reinforced with C-GRID failed in flexural compression shear mode between the supports with bars falling through bond. The poles confined with steel spirals underwent compression failure at the support due to flexure with comparable failure loads.
7. Proposed equations for the calculation of the effective moment of inertia for concrete structures reinforced with FRP bars accurately estimates the deflection of spun concrete poles reinforced with CFRP bars.
8. The ACI 440.1R-03 crack width equation did not accurately predict the test data in some cases. Although the experimental data was limited, it appears that a new ACI equation is needed for round cross-sections.
9. Additional tests with different reinforcement ratios will provide more information that will help in better understanding the flexural behavior of spun concrete poles reinforced with CFRP bars.

ACKNOWLEDGEMENTS

The research was performed in the structures laboratory of the Civil Engineering Department at the University of Alabama at Birmingham. The authors would like to acknowledge Valmont-Newmark Company for their technical and financial support in manufacturing the test specimens for the experimental study. Also, the authors would like to acknowledge TechFab LLC for donating the C-GRID used in this study.

REFERENCES

1. Lyons, P., J., (2003), "Feasibility Study of CFRP Prestressed Spun Cast Concrete Poles for Transmission Line Support," M.S. Thesis, University of Alabama, 2003.
2. Terrasi, G. P., Lees, J. M. (2003), "CFRP Prestressed Concrete Lighting Columns" Field Applications of FRP Reinforcement: Case Studies, ACI, 2003 convention, pp. 55-74
3. Oliphant, W. H., Wong, C. J. (2002), "Spun Concrete Poles for Electrical Transmission Structure Applications – Continuing to Push the Envelope of the Technology" Proceedings of the Electrical Transmission in a New Age Conference, Sept. 9 – Sept. 12, 2002, Omaha, Nebraska, pp. 241-248
4. Fouad, Fouad H., Sherman, Doug, and Werner, Rolf J, (1992), "Spun Prestressed Concrete Poles - Past, Present, and Future," Concrete International, American Concrete Institute, Volume 14, Number 11, November 1992, pp. 25-29.
5. Rodgers, Thomas E., Jr, (1984), "Prestressed Concrete Poles: State-of-the-Art," Journal of the Prestressed Concrete Institute, Vol. 29, No. 5, September-October 1984, pp.52-103.
6. ASTM Standard A82, 2007, "Standard Specification for Steel Wire, Plain, for Concrete Reinforcement" ASTM International, West Conshohocken, PA, www.astm.org.
7. ACI 318-08, (2008), "Building Code Requirements for Structural Concrete" prepared by the ACI committee 318, Jan. 2008
8. ACI 440.1R-03, (2003), "Guide for the Design and Construction of Concrete Reinforced with FRP Bars" prepared by the ACI committee 440, Mar. 2003.
9. ACI 440.1R-06, (2006), "Guide for the Design and Construction of Concrete Reinforced with FRP Bars" prepared by the ACI committee 440.

10. Bischoff, P. H., and Scanlon, A., (2007), "Effective Moment of Inertia for Calculating Deflections of Concrete Members Containing Steel Reinforcement and Fiber-Reinforced Polymer Reinforcement." ACI Structural Journal, Vol. 104, No. 1, pp. 68-75.
11. PCI Committee on Prestressed Concrete Poles, (1997), "Guide for the Design of Prestressed Concrete Poles," PCI Journal, Vol. 42, No. 6, Nov.-Dec. 1997, pp. 94-134.
12. Yost, J. R., Gross, S. P., and Dinehart, D. W. (2003), "Effective Moment of Inertia for Glass Fiber-Reinforced Polymer Reinforced Concrete Beams." ACI Structural Journal, Vol. 100, No. 6, pp. 732-739.
13. Shalaby, Ashraf, (2007), "Development of a New Spun Concrete Pole Reinforced with Carbon Fiber Reinforced Polymer Bars." Ph.D. Dissertation, University of Alabama at Birmingham, 2007

NOTATIONS

α_b	Bond coefficient for the effective moment of inertia calculation
β_d	Reduction coefficient
Δ	Deflection of the pole
A	Effective tension area of concrete defined as the area of concrete having the same centroid as that of the farthest tensile reinforcement from the neutral axis
A_{fi}	Area of the i^{th} reinforcement
c	Location of the neutral axis measured from the extreme compression fiber of the pole
d_c	The distance from the centroid of the effective tensions area of concrete to the extreme tensile fiber of the cross-section
d_i	Distance of the i^{th} reinforcement from the extreme compression fiber
E_c	Modulus of elasticity of concrete
E_f	Modulus of elasticity of FRP bars
E_s	Modulus of elasticity of steel
e_i	Distance of the i^{th} reinforcement to the neutral axis
f'_c	Cylinder compressive strength of concrete at 28 days
f_{fei}	Stress of the i^{th} reinforcement
f_{fu}	Ultimate strength of the CFRP bars

f_r	Modulus of rupture of concrete
I	Moment of inertia of the cross-section
I_{A_a}	Moment of inertia of annulus at the neutral axis
I_{cr}	Cracking moment of inertia
I_e	Effective moment of inertia of the cross-section
I_g	Gross moment of inertia of the section
k_b	Bond coefficient for calculation of the crack width
Kc	Position of the centroid of the stress block
L	Length of the pole
M	Applied moment
M_a	Maximum moment subjected to the pole
M_{cr}	Cracking moment of concrete
M_u	Ultimate moment capacity of the section
n_f	Modular ratio between CFRP and concrete
w	Crack width in mils
y_t	Distance from the centroidal axis to the extreme tensile fiber of the section
x	Distance from the support

ABOUT THE AUTHOR

Ashraf M Shalaby, Ph.D, Research Assistant, Department of Civil, Construction, and Environmental Engineering, University of Alabama at Birmingham, Birmingham, AL, USA



Fouad H Fouad, Ph.D, P.E., Chair and Professor, Department of Civil, Construction, and Environmental Engineering, University of Alabama at Birmingham, Birmingham, AL, USA. Dr. Fouad is a fellow of ACI and ASCE, and chairman of the PCI Committee on Prestressed Concrete Poles.



Ronald Albanese, P.E., MSCE, Senior Engineer, Valmont-Newmark, Birmingham, AL, USA. Member of the PCI Committee on Prestressed Concrete Poles.



SYNOPSIS

Prestressed spun concrete poles are used primarily for supporting electric power transmission lines and distribution and for area lighting. It is common to have them placed in aggressive environments, and in many applications they are placed directly in brackish or saltwater, resulting in deterioration of the concrete pole due to steel corrosion. A new type of reinforcement that can provide the desired structural characteristics and at the same time address the issue of corrosion is needed. Carbon Fiber-Reinforced Polymer (CFRP) composites are showing immense potential as a replacement to steel reinforcement due to their corrosion resistance, very high strength, and lighter weight compared to steel, which enables easier handling and reduces the self weight of structures. This research work presents an experimental and analytical program that evaluates the flexural behavior of spun concrete poles reinforced with CFRP bars. The results of the study showed that the performance of the poles reinforced with CFRP bars was satisfactory under bending loads, which are the primary governing loads in most applications.

KEYWORDS

Concrete Poles; Carbon fiber reinforced polymers; FRP; Flexure Behavior; Deflection; Moment Capacity; Crack Width

FIGURE CAPTIONS

Figure 1: Aslan 200 CFRP rebar sample

Figure 2: C-GRID CFRP grid sample

Figure 3: Specimen concrete dimensions

Note: 1in = 25.4 mm

Figure 4: Pole confined with steel spiral

Figure 5: Pole confined with C-GRID

Figure 6: Specimen cross-sectional details

Note: 1in = 25.4 mm

Figure 7: Schematic diagram showing the test setup

Figure 8: Details of pole end supports

Figure 9: The clamp fixation of the supporting beams

Figure 10: The loading system at pole tip end

Figure 11: Strain gages location at 6 in and 18 in from the support

Figure 12: Deflection measurement at pole tip end

Figure 13: LVDTs for deflection measurements and corrections

Figure 14: Load deflection curve of the four specimens

Note: 1in = 25.4 mm 1lbs = 4.45 N

Figure 15: Load deflection curve of the four specimens up to a load of 1700 lbs

Note: 1in = 25.4 mm 1lbs = 4.45 N

Figure 16: Concrete crushing at failure for poles confined with steel spirals

Figure 17: Concrete failure for poles confined with C-GRID

Figure 18: Slippage of CFRP bars at failure of poles confined with C-GRID

Figure 19: Cracking pattern for pole P01-6SS

Figure 20: Cracking pattern for pole P03-12SS

Figure 21: Crack width versus loading

Note: 1 mil = 0.0254 mm 1lbs = 4.45 N

Figure 22: Concrete stress area and assumed stress distribution in pole section

Figure 23: Crack width parameters for pole specimens

Figure 24: Load-deflection curve for the poles reinforced with 6 CFRP bars

Note: 1in = 25.4 mm 1lbs = 4.45 N

Figure 25: Load-deflection curve for the poles reinforced with 12 CFRP bars

Note: 1in = 25.4 mm 1lbs = 4.45 N

Figure 26: Load-crack width curve for poles reinforced with 6 CFRP bars

Note: 1 mil = 0.0254 mm 1lbs = 4.45 N

Figure 27: Load-crack width curve for poles reinforced with 12 CFRP bars

Note: 1 mil = 0.0254 mm 1lbs = 4.45 N

TABLES

Table 1: Physical properties of CFRP Aslan 200

Bar Dia. (in)	Cross-Sectional Area (in ²)	Nominal Diameter (in)	Tensile Strength (ksi)	Tensile Modulus of Elasticity (psi 10 ⁶)	Ultimate Strain (%)
#3	0.1010	0.362	300	18	1.7

Note: 1in = 25.4 mm 1in² = 645 mm² 1000 psi = 6.89 MPa

Table 2: Typical properties of CFRP C-GRID

Grid Designation	Longitudinal Properties		Transverse Properties	
	Strand Spacing (in)	Grid Strength (kips/ft)	Strand Spacing (in)	Grid Strength (kips/ft)
C50-2.9x2.9	2.9	4.9	2.9	3.9

Note: 1in = 25.4 mm 1ft = 305 mm 1kips = 4.45 kN

Table 3: Strand physical properties of CFRP C-GRID

Grid Designation	Tensile Strength (ksi)	Tensile Modulus of Elasticity (psi 10 ⁶)	Ultimate strain (%)	Longitudinal Cross- sectional Area (in ²)	Transverse Cross- sectional Area (in ²)
C50-2.9x2.9	340	34	1.0	0.0036	0.00312

Note: 1in² = 645 mm² 1000 psi = 6.89 MPa

Table 4: Experimental program and specimen details

Specimen ID	No. of Bars	Bar Dia. (in)	Bar Type	Spiral Reinforcement	Conc. Cover (in)	Pole Outer Dia. (in)		Pole Inner Dia. (in)		Pole Length (ft)	Conc. Strength (psi)
						At Tip	At Butt	At Tip	At Butt		
P01-6SS	6	3/8	CFRP	W2.9 @ 3"	0.75	8.91	13.23	3.91	7.75	20	11,000
P02-6CG				C50-2.9x2.9							
P03-12SS	12	3/8	CFRP	W2.9 @ 3"	0.75	8.91	13.23	3.91	7.75	20	11,000
P04-12CG				C50-2.9x2.9							

Note: 1in = 25.4 mm 1ft = 305 mm 1000 psi = 6.89 MPa

Table 5: Summary of test results

Specimen ID.	No. of Bars	Cracking Load (lbs)	Tip Deflection at Cracking (in)	Cracking Strain (10^{-6})	Failure Load (lbs)	Corrected Tip Deflection at Failure (in)	Concrete Compressive Failure Strain (10^{-4})	Max. Concrete Compressive Strain (10^{-4})
P01-6SS	6	568	0.59	97	3790	25.84	32.06	35.58
P02-6CG		1025	1.54	170	4102	25.91	NA	24.96
P03-12SS	12	545	1.08	96	4247	20.465	NA	23.05
P04-12CG		904	0.92	106	5251	21.99	26.44	26.44

Note: 1in = 25.4 mm 1lbs = 4.45 N

Table 6: Failure modes of the poles

Specimen ID.	Failure Mode
P01-6SS	Compression failure at fulcrum support
P02-6CG	Diagonal tensions shear failure between supports combined with compression shear failure at fulcrum support
P03-12SS	Compression failure at fulcrum support
P04-12CG	Diagonal tensions shear failure between supports combined with compression shear failure at fulcrum support

Table 7: Theoretical and experimental cracking moments at 6 in from the fulcrum support

Specimen ID.	Theoretical Cracking Moment (ft.kips)	Experimental Cracking Moment (ft.kips)	% Difference
P01-6SS	11.46	9.09	26%
P02-6CG	11.46	16.40	(30%)
P03-12SS	11.46	8.72	31%
P04-12CG	11.46	14.46	(21%)
Average	11.46	12.17	(6%)

Note: 1ft.kips = 1.36 kN.m

Table 8: Theoretical and experimental ultimate moments at fulcrum support

Specimen ID.	Theoretical Ultimate Moment (ft.kips)	Experimental Ultimate Moment (ft.kips)	% Difference
P01-6SS	59.48	60.64	(2%)
P02-6CG	59.48	65.63	(9%)
P03-12SS	74.25	67.95	9%
P04-12CG	74.25	84.02	(12%)

Note: 1ft.kips = 1.36 kN.m

Table 9: Theoretical and experimental maximum crack width

Specimen ID	Load (lbs)	% from Ultimate Load	Crack Width (mils)	
			Experimental	Theoretical
P01-6SS	After Unloading	NA	40	50
P02-6CG	2854	70%	60	50
P03-12SS	3342	77%	35	35
P04-12CG	3393	65%	20	36

Note: 1 mil = 0.0254 mm 1lbs = 4.45 N



Figure 1: Aslan 200 CFRP rebar sample



Figure 2: C-GRID CFRP grid sample

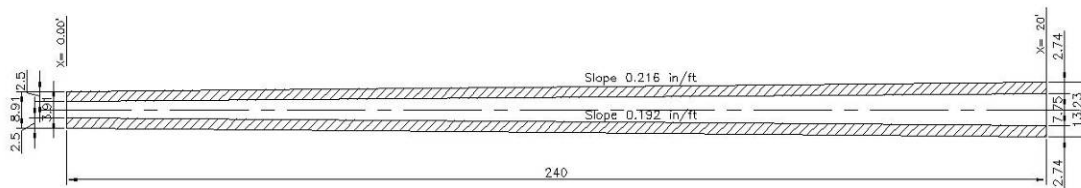


Figure 3: Specimen concrete dimensions

Note: 1in = 25.4 mm

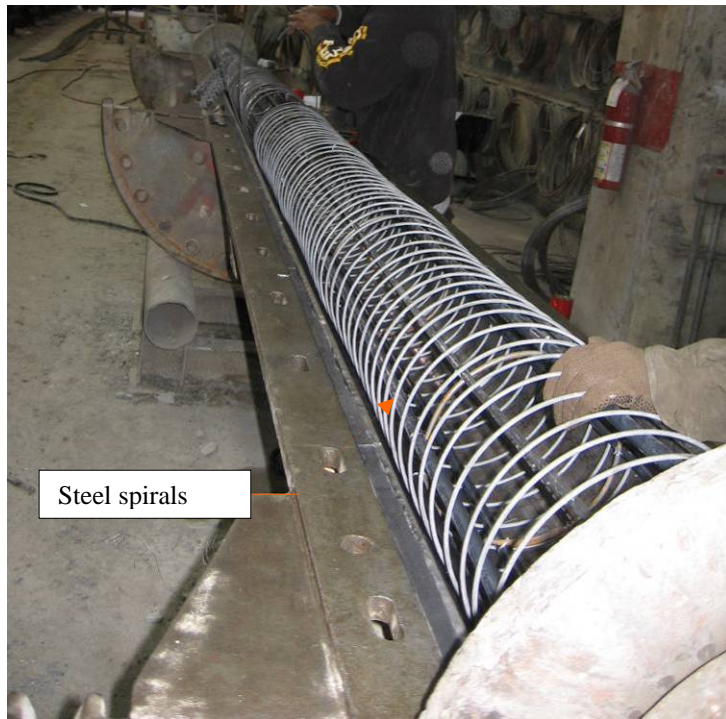


Figure 4: Poles confined with steel spirals

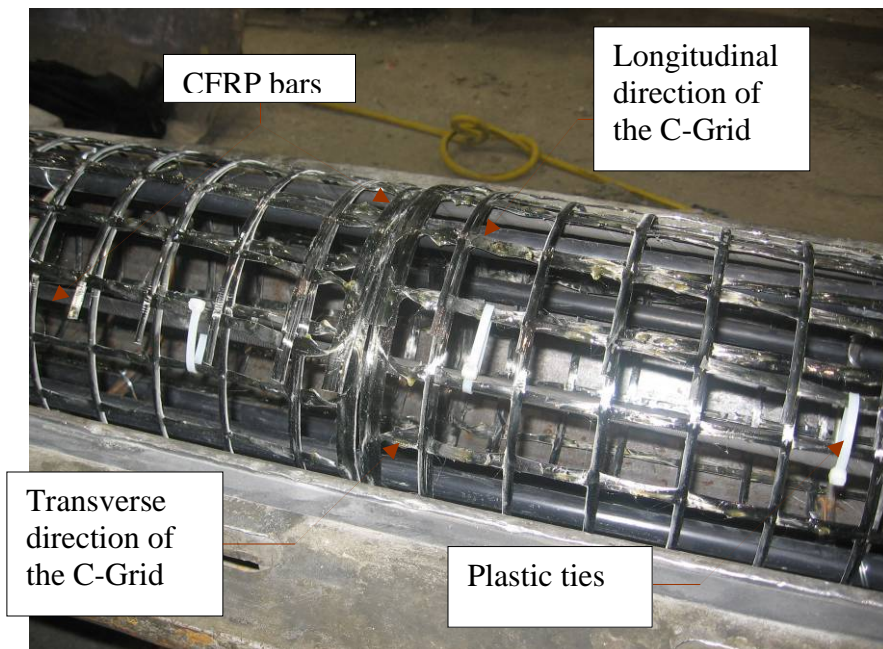


Figure 5: Poles confined with C-GRID

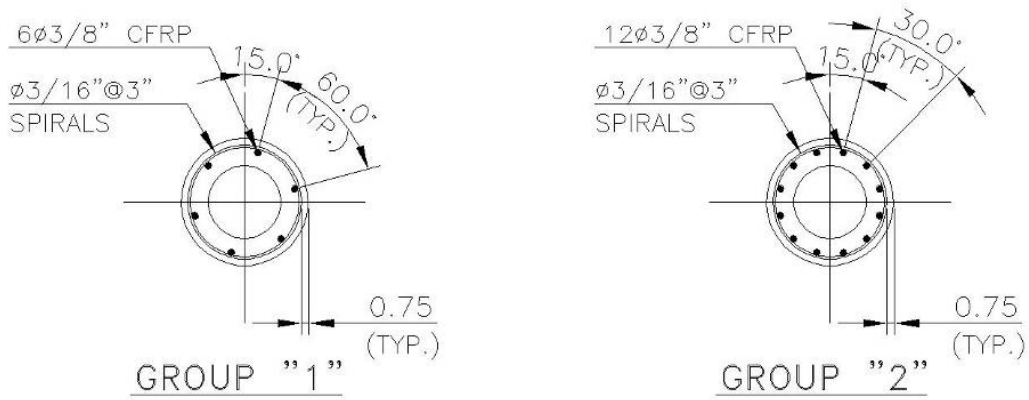


Figure 6: Specimen cross-sectional details

Note: 1in = 25.4 mm

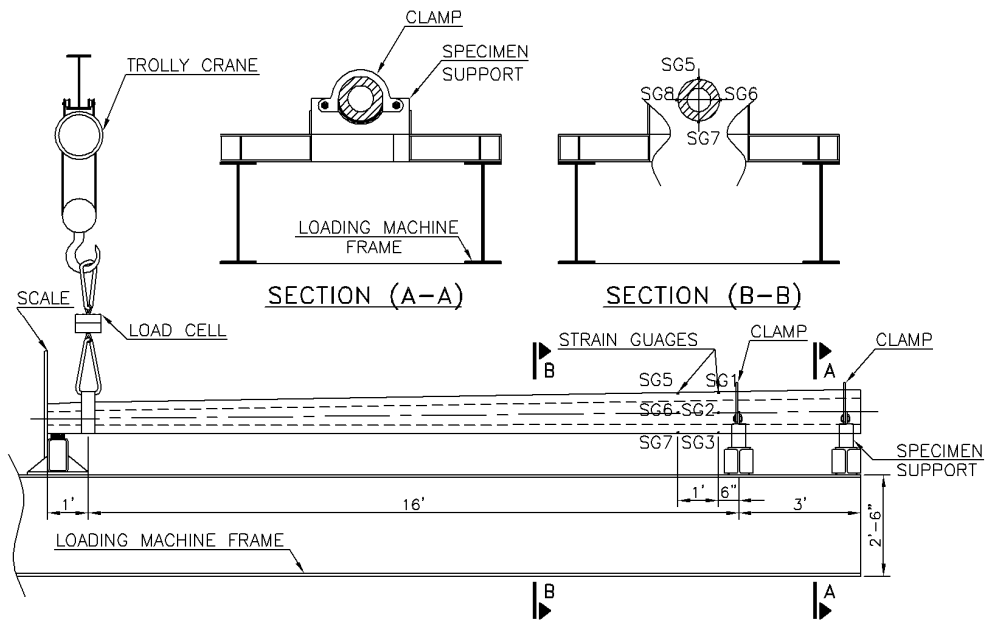


Figure 7: Schematic diagram showing the test setup

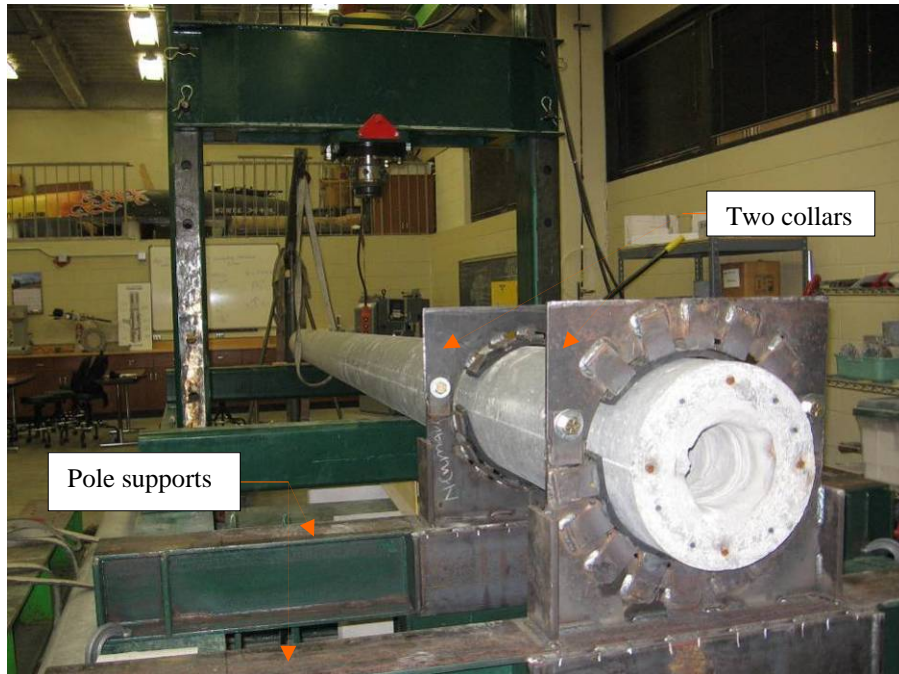


Figure 8: Details of pole end supports

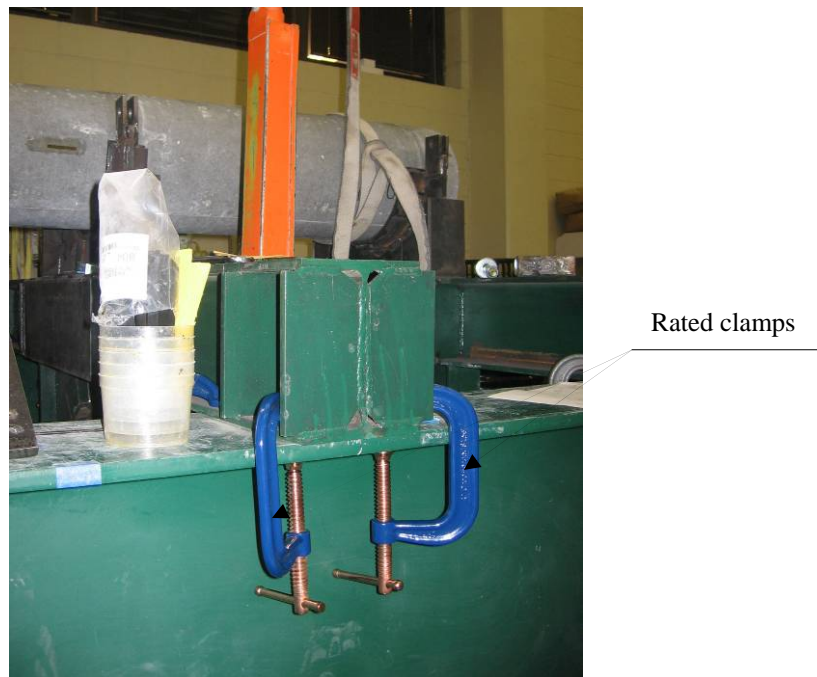


Figure 9: The clamp fixation of the supporting beams

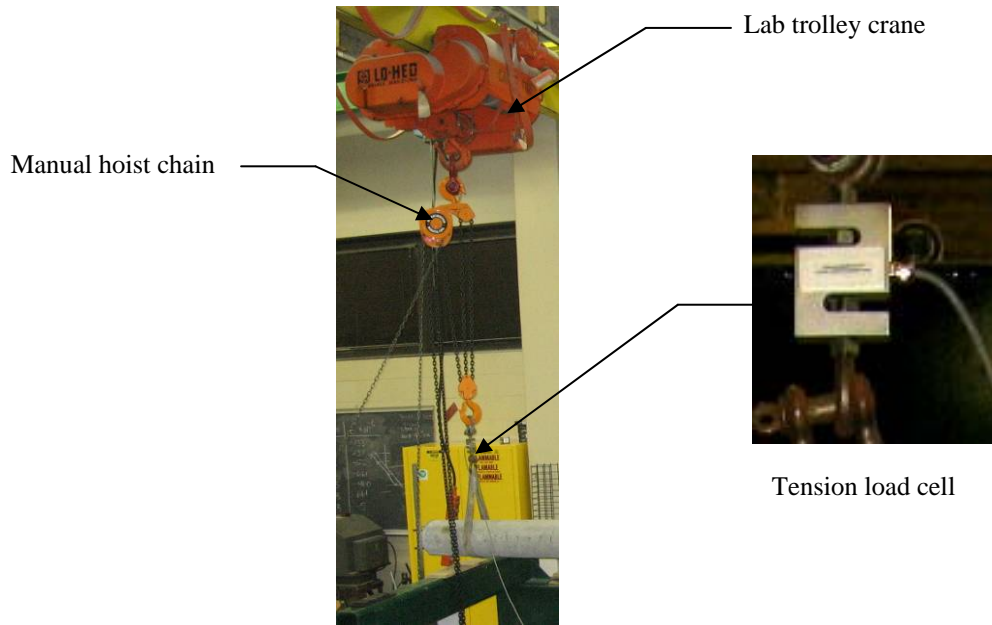


Figure 10: The loading system at pole tip end



Figure 11: Strain gages location at 6 in and 18 in from the support

Measuring Tape



Measuring Scale



Figure 12: Deflection measurement at pole tip end



Figure 13: LVDTs for deflection measurements and corrections

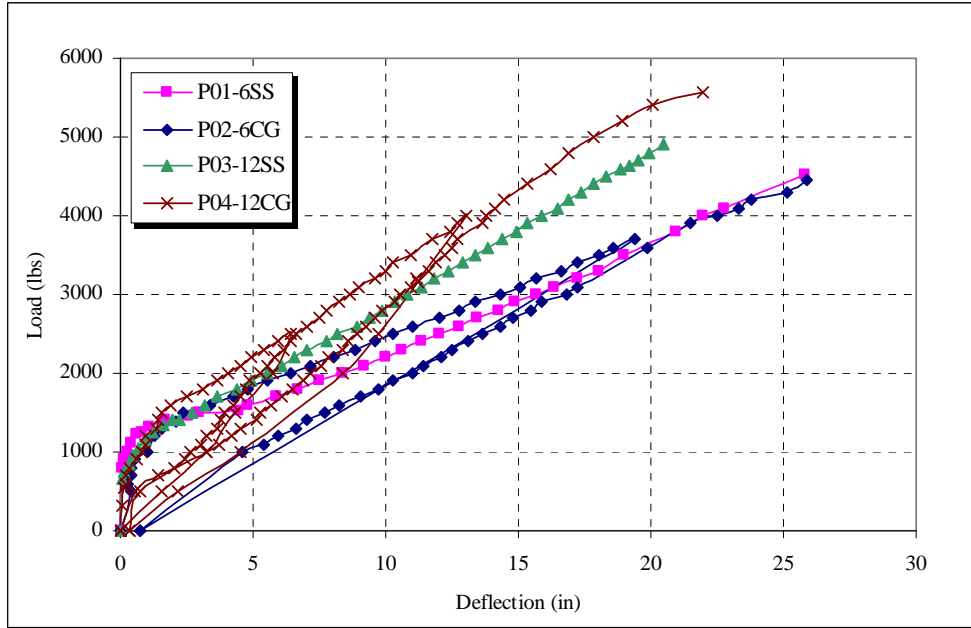


Figure 14: Load deflection curve of the four specimens

Note: 1in = 25.4 mm 1lbs = 4.45 N

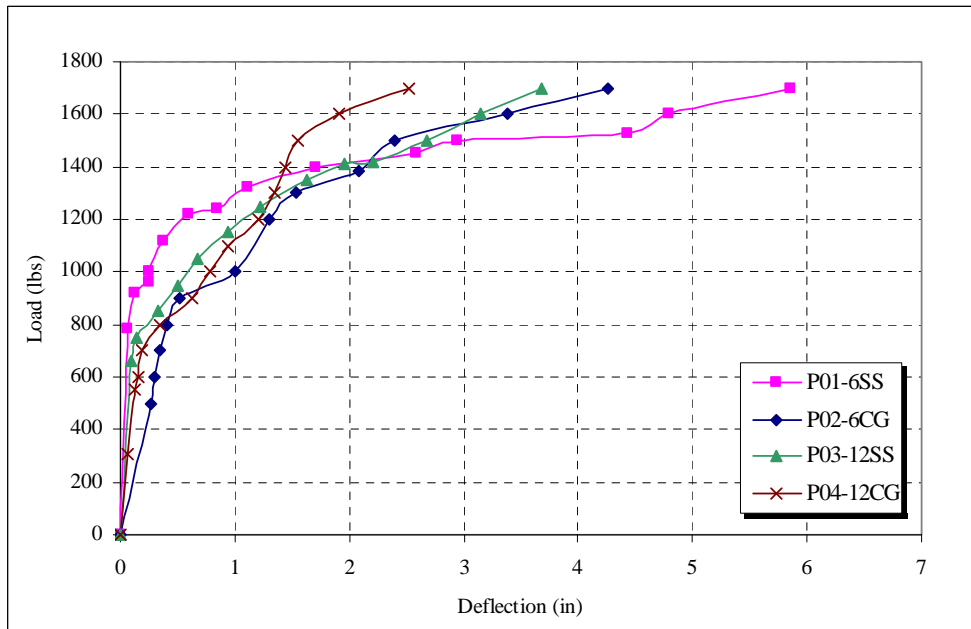


Figure 15: Load deflection curve of the four specimens up to a load of 1700 lbs

Note: 1in = 25.4 mm 1lbs = 4.45 N

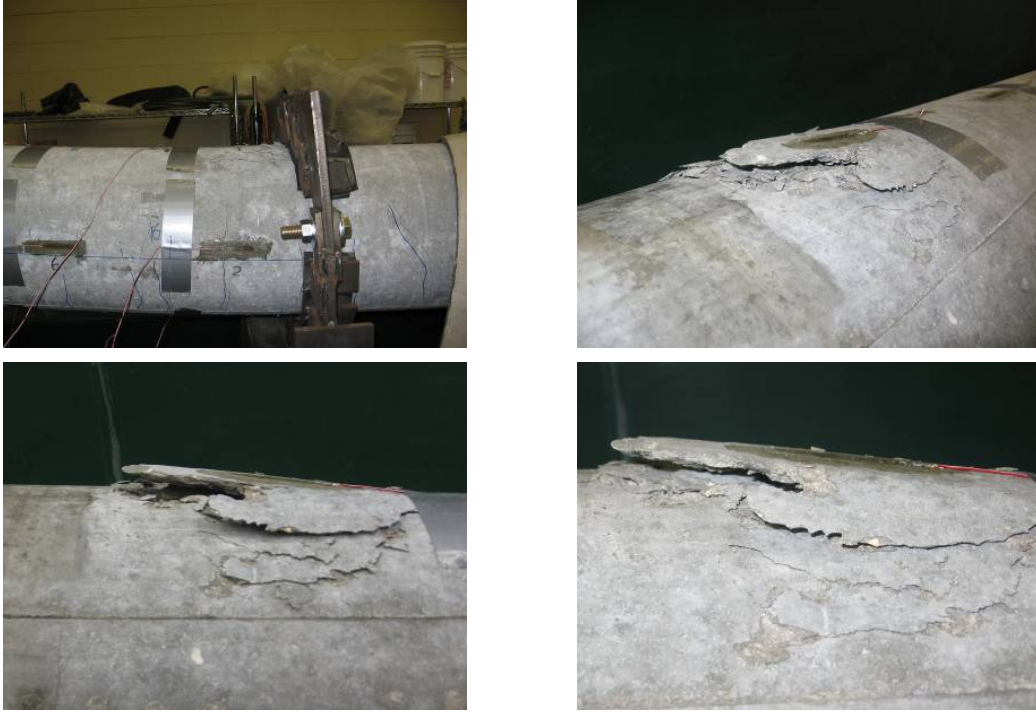


Figure 16: Concrete crushing at failure for poles confined with steel spirals



Figure 17: Concrete failure for poles confined with C-GRID



Figure 18: Slippage of CFRP bars at failure of poles confined with C-GRID

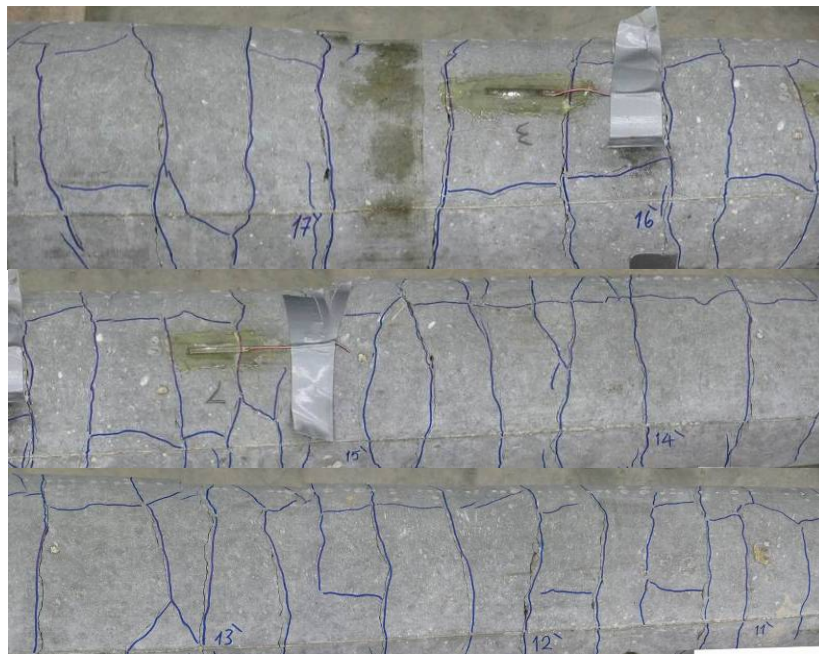


Figure 19: Cracking pattern for pole P01-6SS

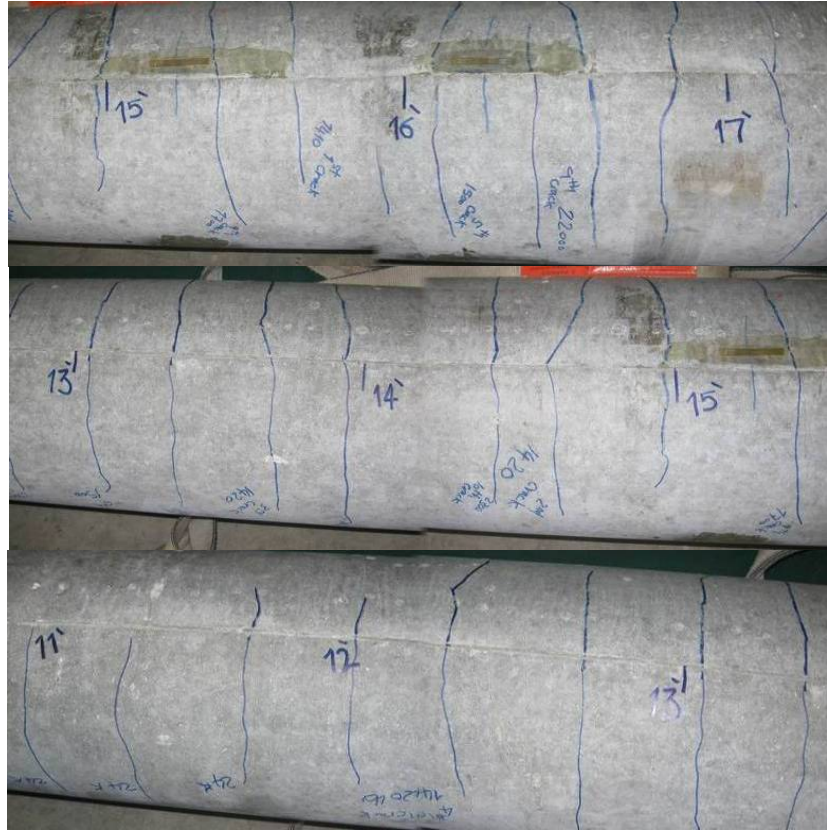


Figure 20: Cracking pattern for pole P03-12SS

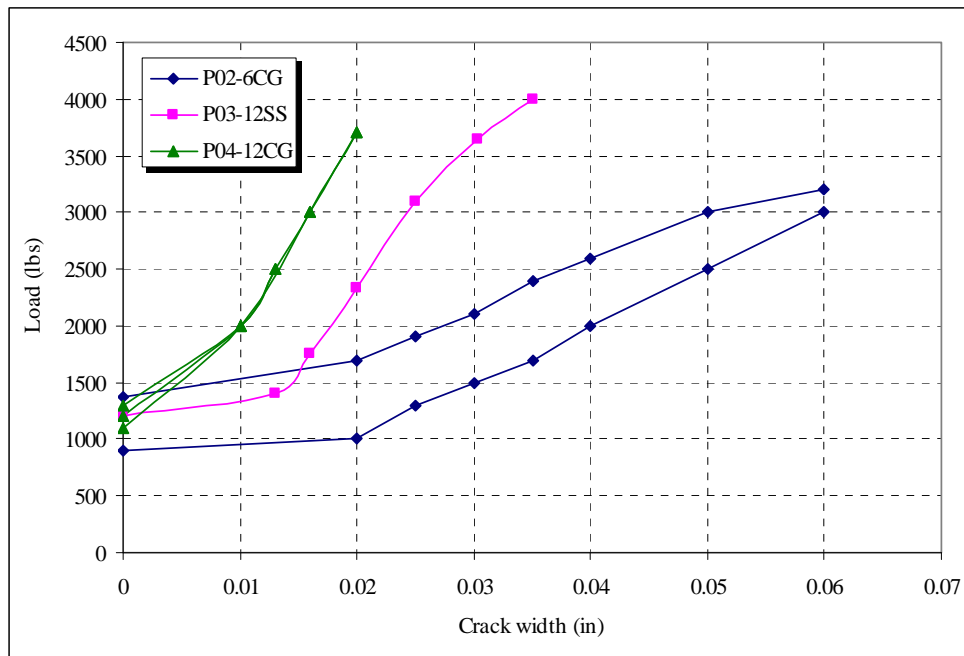


Figure 21: Crack width versus loading

Note: 1in = 25.4 mm 1lbs = 4.45 N

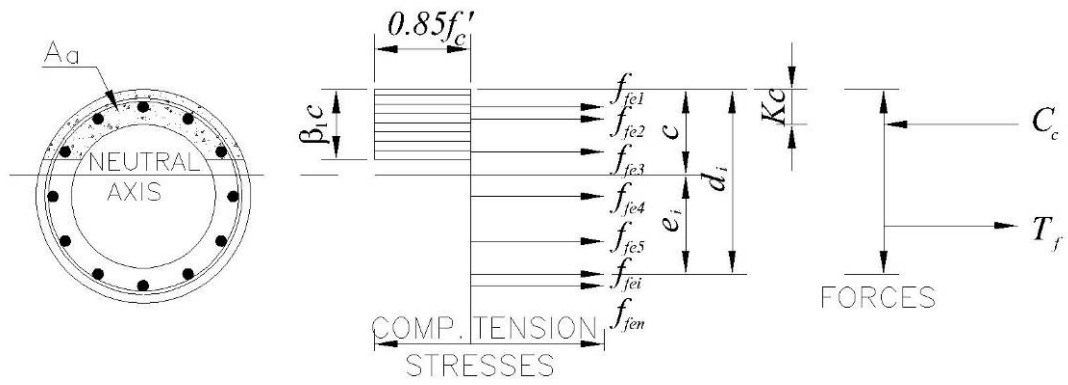


Figure 22: Concrete stress area and assumed stress distribution in pole section

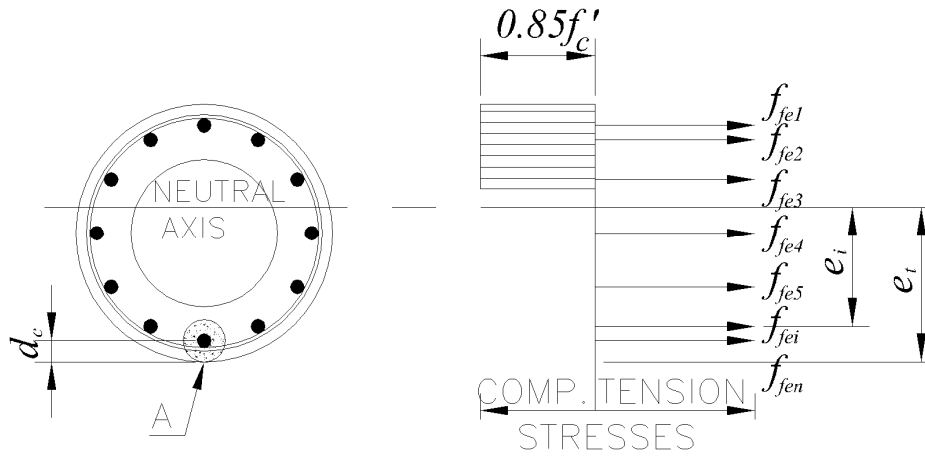


Figure 23: Crack width parameters for pole specimens

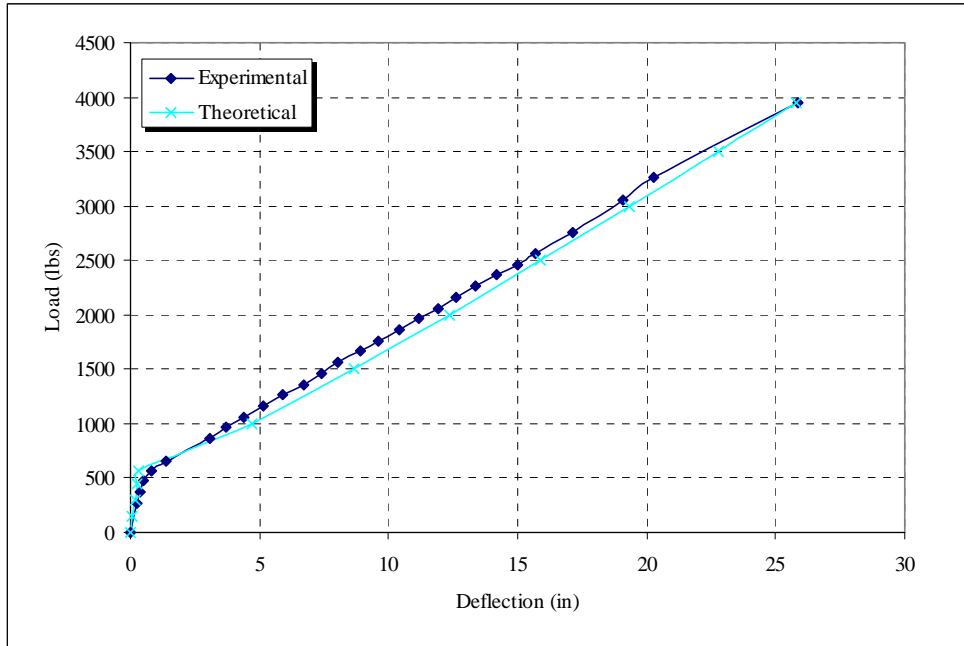


Figure 24: Load-deflection curve for poles reinforced with 6 CFRP bars
 Note: 1in = 25.4 mm 1lbs = 4.45 N

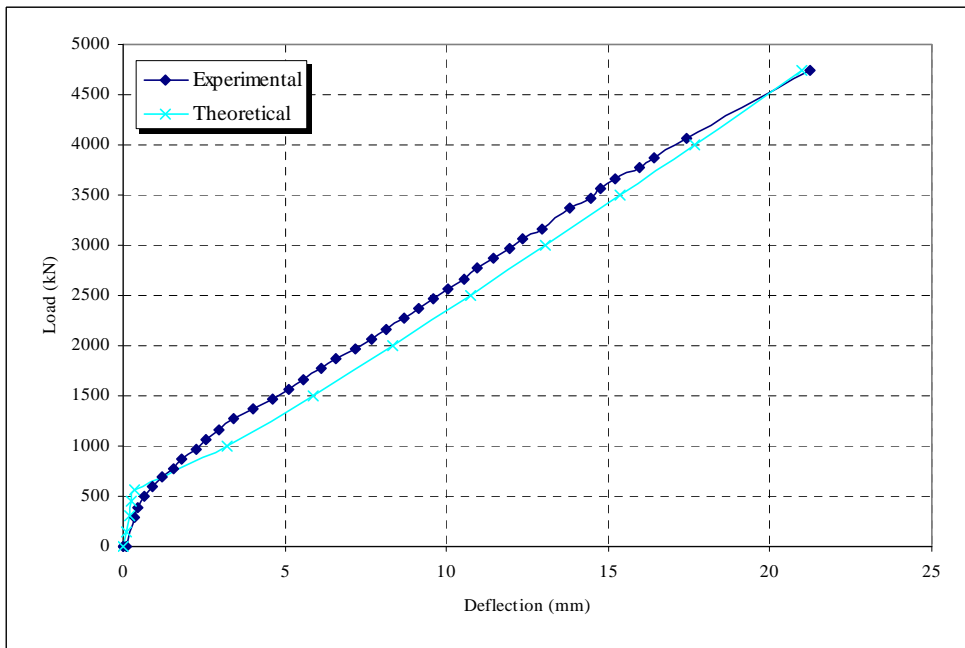


Figure 25: Load-deflection curve for poles reinforced with 12 CFRP bars
 Note: 1in = 25.4 mm 1lbs = 4.45 N

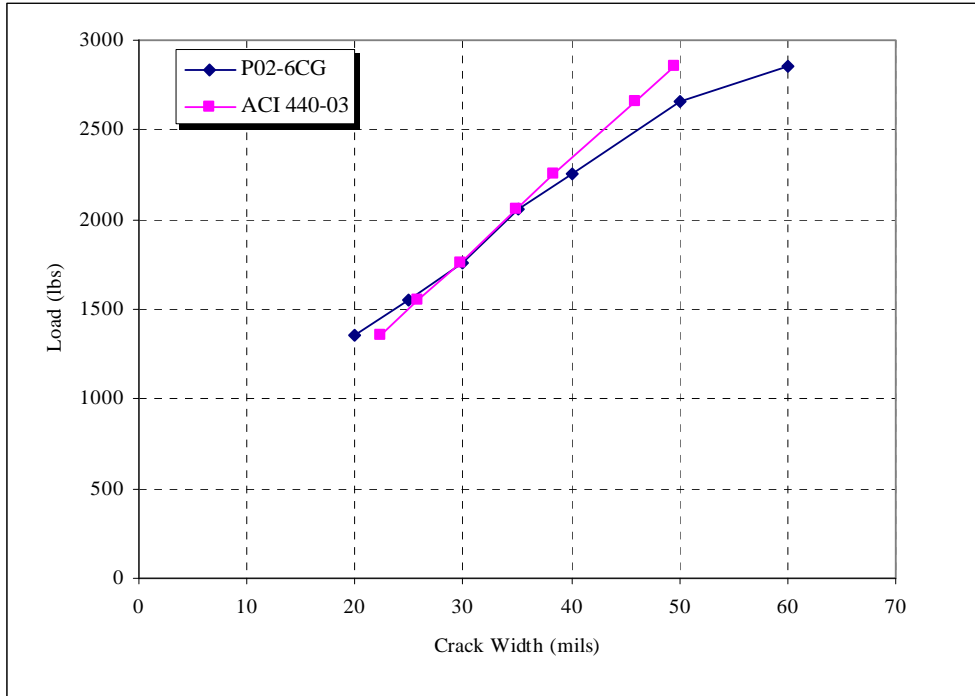


Figure 26: Load-crack width curve for poles reinforced with 6 CFRP bars
 Note: 1 mil = 0.0254 mm 1lbs = 4.45 N

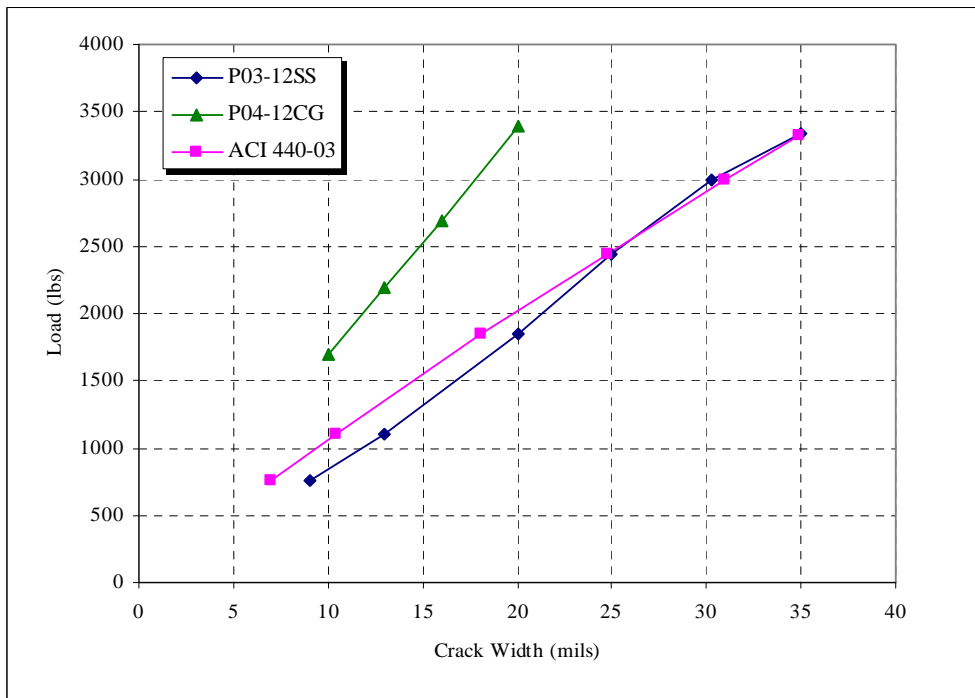


Figure 27: Load-crack width curve for poles reinforced with 12 CFRP bars
 Note: 1 mil = 0.0254 mm 1lbs = 4.45 N